Modelling the dwarf Spheroidals: Cores, Cusps and orbital structure

Nicola Cristiano Amorisco

with Prof. Wyn Evans

Institute of Astronomy
University of Cambridge

7th June 2012
Workshop CIAS Meudon 2012

dSphs and Near-Field Cosmology

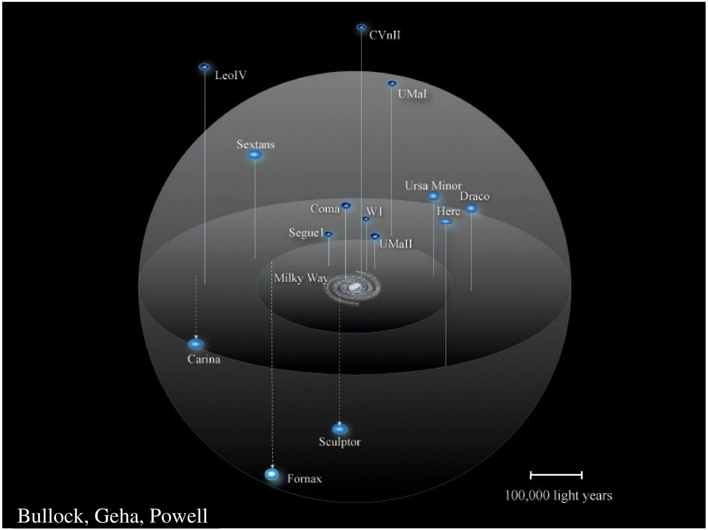

dSphs and GCs

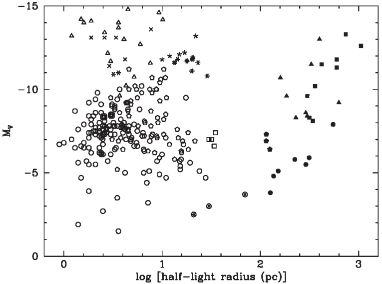

Gilmore et al. 2007

Omega Centauri

Sculptor

dSphs and GCs

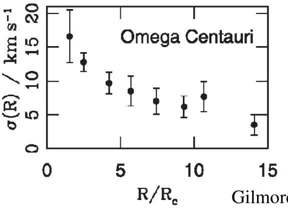

Gilmore et al. 2007

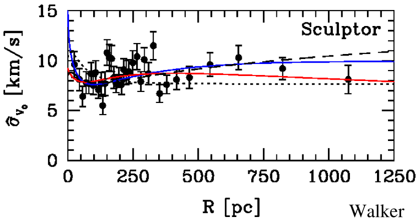

Walker et al. 2009

mass does not follow light:

dSphs are the most dark matter dominated systems known, a unique testing ground for cosmology

dSphs and GCs

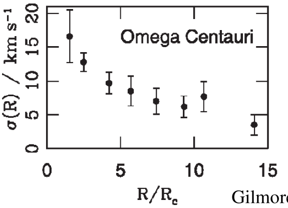

Gilmore et al. 2007

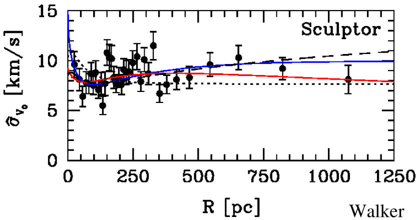

Walker et al. 2009

mass does not follow light:

dSphs are the most dark matter dominated systems known,
a unique testing ground for cosmology

Dynamics and Near-Field Cosmology

dark halo

- mass profile?
- core or cusp?
- concentration?
- phase-space structure?

stellar populations

- orbital structure?
- evolutionary history?
- accreted/expelled gas?
- baryonic feedback?

Because of degeneracies,
it has not proved easy to address these questions.

Mass-Anisotropy degeneracy

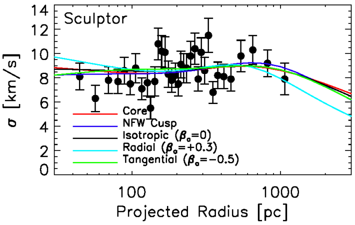

Walker 2012

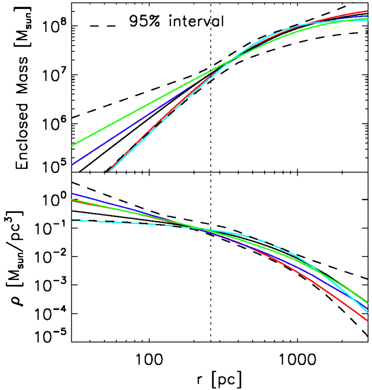

1 - Jeans' Pitfall

- luminous density ρ_*
- gravitational potential Φ
- orbital structure β

Solve the Jeans' eq. and calculate the LOS kinematic profile

$$\sigma^2_{LOS}(R) = \frac{2}{\Sigma_*(R)} \int_R^\infty r dr \left(1 - \beta \frac{R^2}{r^2}\right) \frac{\rho_* \sigma_r^2}{\sqrt{r^2 - R^2}}$$

1 - Jeans' Pitfall

- luminous density ρ_*
- gravitational potential Φ
- orbital structure β

Solve the Jeans' eq. and calculate the LOS kinematic profile

$$\sigma^2_{LOS}(R) = \frac{2}{\Sigma_*(R)} \int_R^\infty r dr \left(1 - \beta \frac{R^2}{r^2}\right) \frac{\rho_* \sigma_r^2}{\sqrt{r^2 - R^2}}$$

1 - Jeans' Pitfall

- luminous density ρ_*
- gravitational potential Φ
- orbital structure β

Solve the Jeans' eq. and calculate the LOS kinematic profile

$$\sigma^2_{LOS}(R) = \frac{2}{\Sigma_*(R)} \int_R^\infty r dr \left(1 - \beta \frac{R^2}{r^2}\right) \frac{\rho_* \sigma_r^2}{\sqrt{r^2 - R^2}}$$

1 - Jeans' Pitfall

- luminous density ρ_*
- gravitational potential Φ
- orbital structure β

Solve the Jeans' eq. and calculate the LOS kinematic profile

$$\sigma^2_{LOS}(R) = \frac{2}{\Sigma_*(R)} \int_R^\infty r dr \left(1 - \beta \frac{R^2}{r^2}\right) \frac{\rho_* \sigma_r^2}{\sqrt{r^2 - R^2}}$$

1 - Jeans' Pitfall

$$\left.\begin{array}{cc} \text{luminous density} & \rho_* \\ \text{halo potential} & \Phi \\ \text{orbital structure} & \beta \end{array}\right\}$$ are NOT independent quantities

Not all combinations guarantee $f \geq 0$!

$$\left.\begin{array}{c} \text{Plummer or King} \\ \text{any cusped halo} \\ \text{isotropic} \end{array}\right\}$$ is NOT a physical model (Ciotti & Pellegrini 1992, An & Evans 2009)

- this introduces an artificial degeneracy
- no prediction for Σ_*

1 - Jeans' Pitfall

$$\left.\begin{array}{cc} \text{luminous density} & \rho_* \\ \text{halo potential} & \Phi \\ \text{orbital structure} & \beta \end{array}\right\}$$

are NOT
independent quantities

Not all combinations guarantee $f \geq 0$!

$$\left.\begin{array}{c} \text{Plummer or King} \\ \text{any cusped halo} \\ \text{isotropic} \end{array}\right\}$$

is NOT a physical model
(Ciotti & Pellegrini 1992,
An & Evans 2009)

- this introduces an artificial degeneracy
- no prediction for Σ_*

1 - Jeans' Pitfall

$$\left.\begin{array}{cc} \text{luminous density} & \rho_* \\ \text{halo potential} & \Phi \\ \text{orbital structure} & \beta \end{array}\right\}$$ are NOT independent quantities

Not all combinations guarantee $f \geq 0$!

$$\left.\begin{array}{c} \text{Plummer or King} \\ \text{any cusped halo} \\ \text{isotropic} \end{array}\right\}$$ is NOT a physical model (Ciotti & Pellegrini 1992, An & Evans 2009)

- this introduces an artificial degeneracy
- no prediction for Σ_*

2 - Multiple stellar populations

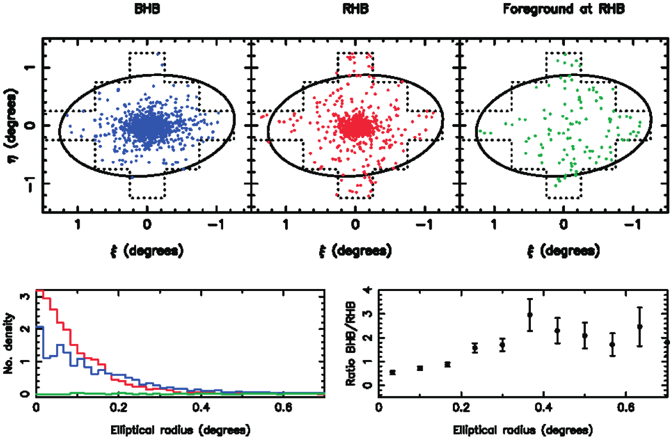

Sculptor: Tolstoy et al. 2004

3 - Unused data: Line Profiles

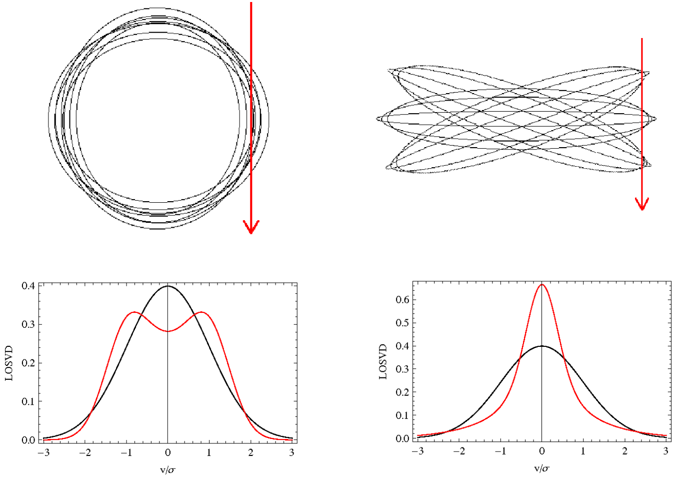

LOSVDs are the imprint of orbital structure.

Cores from multiple stellar pops

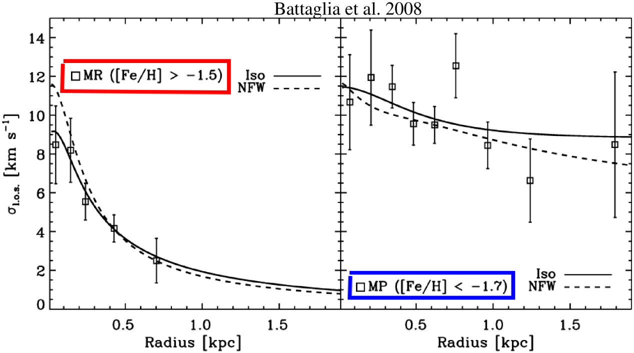

Jeans' modelling in Sculptor for MP and MR stellar populations.

- Marginal preference for a core
- NFW fit still statistically acceptable

Cores from mass estimators

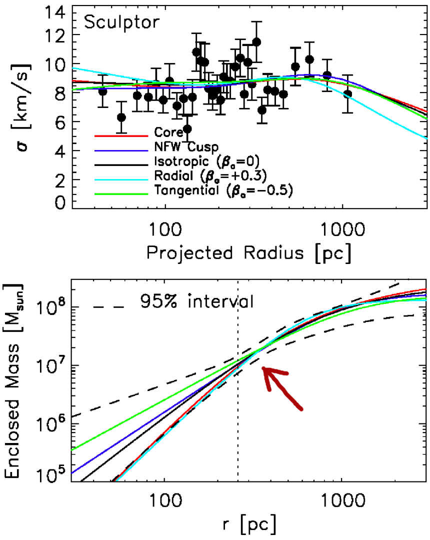

Mass estimator

$$M(R_h) \approx K \frac{R_h \sigma_{los}^2}{G}$$

Walker et al. 2009,
Wolf et al. 2010,

Amorisco & Evans 2011

Cores from mass estimators

Walker & Penarrubia 2011

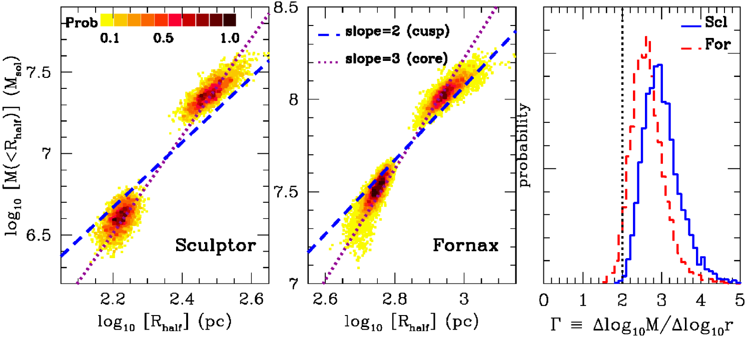

- significant improvement: metallicity distribution
- not a dynamical model: detailed information on the halo? orbital structure?

Cores from phase-space modelling

We adopt the observables as in Battaglia et al. 2008

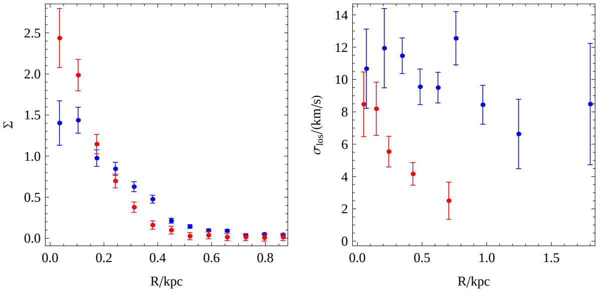

MP: [Fe/H] < -1.7 MR: [Fe/H] > -1.5

The phase-space approach gives a prediction for both kinematics and photometry.

Choice of the Distribution Function

What level of complexity do we need?

$$f_* \propto \exp\left[\frac{\Phi(r_t) - E}{\sigma^2}\right] - 1$$

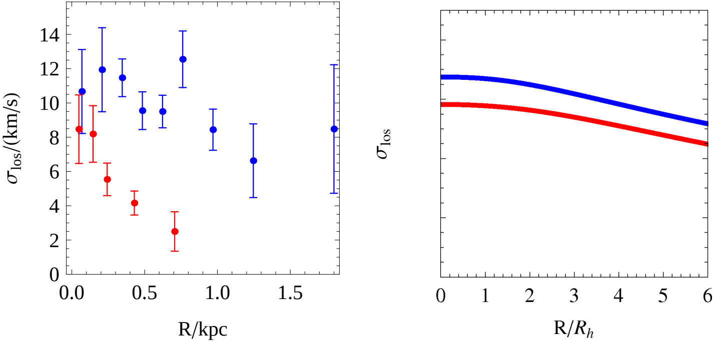

The tidal cut is incompatible with the MR stellar population.

Choice of the Distribution Function

What level of complexity do we need?

$$f_* \propto \exp\left[\frac{\Phi(r_t) - E}{\sigma^2}\right] - 1$$

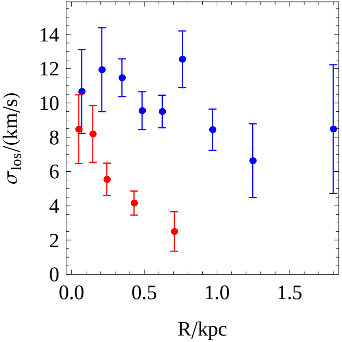

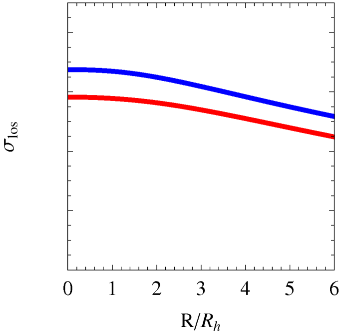

The tidal cut is incompatible with the MR stellar population.

Choice of the Distribution Function

The energy-cut in phase-space of the MR population is not tidal in origin. Possibly depending on the original gas distribution.

Hence, we allow for different truncations.

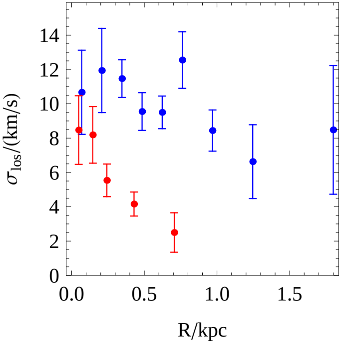

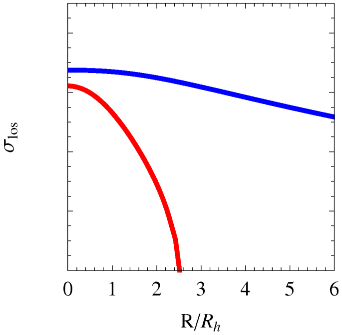

Choice of the Distribution Function

Also, isotropic models are not enough, and a mild radial anisotropy is needed:

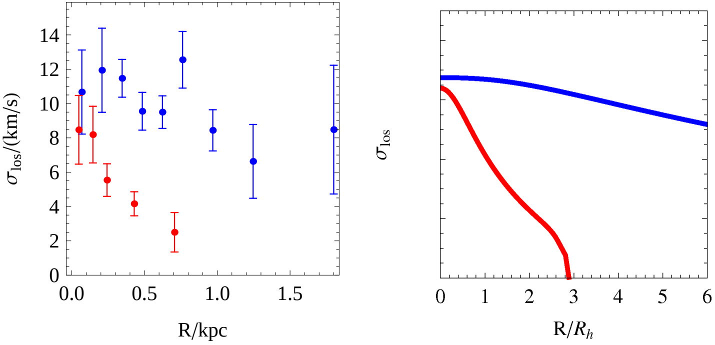

Choice of the Distribution Function

Michie-King DFs:

$$f_* = f_{\rm MK}(E,L) \propto \exp\left(\frac{-L^2}{2r_{\rm a}^2\sigma^2}\right)\left\{\exp\left[\frac{\Phi(r_{\rm t})-E}{\sigma^2}\right]-1\right\}$$

These can cover a wide range of dependences on Energy

- from the **isothermal limit**: $f_* \sim \exp(-E)$
- up to **strongly truncated** systems: $f_* \sim (\Phi(r_{\rm t})-E)$

This is equivalent to an ordering in the ratio $r_{\rm t}/R_{\rm h}$.

Isotropic in the center with an adjustable degree of radial anisotropy at larger radii.

Each stellar population has 3 free parameters:

$$(R_{\rm h}, r_t, \bar{\beta} \equiv \beta(R_{\rm h}))$$

Halo density profile

- the usual **NFW profile**

$$\rho(r) = \frac{\rho_0}{\left(\frac{r}{r_0}\right)\left(1 + \frac{r}{r_0}\right)^2}$$

- an intermediate cusp

$$\rho(r) = \frac{\rho_0}{\left(\frac{r}{r_0}\right)^{1/2}\left(1 + \frac{r}{r_0}\right)^{3/2}}$$

- a **cored halo**

$$\rho(r) = \frac{\rho_0}{\left(1 + \left(\frac{r}{r_0}\right)^2\right)^{3/2}}$$

Maximum-likelihood Analysis

For each parametrization of the dark halo we have 8 free parameters:

$$(r_0, \rho_0; \hat{R}_{\rm h}, \hat{r}_{\rm t}, \bar{\beta}; \hat{R}_{\rm h}, \hat{r}_{\rm t}, \bar{\beta})$$

We consider the likelihood

$$L_{\rm tot} = L_{\rm MP}(r_0, \rho_0; \hat{R}_{\rm h}, \hat{r}_{\rm t}, \bar{\beta}) \cdot L_{\rm MR}(r_0, \rho_0; \hat{R}_{\rm h}, \hat{r}_{\rm t}, \bar{\beta})$$

$$\chi_{\rm tot} = \chi^2_{\rm MP} + \chi^2_{\rm MR}$$

For each population

$$\chi^2 = \chi^2_{\Sigma} + \chi^2_{\sigma}$$

$$\chi^2_{\rm MP} = \chi^2_{\Sigma} + \chi^2_{\sigma} + \chi^2_{r_{\rm t}}$$

Maximum-likelihood Analysis

For each parametrization of the dark halo we have 8 free parameters:

$$(r_0, \rho_0; \hat{R}_{\rm h}, \hat{r}_{\rm t}, \bar{\beta}; \hat{R}_{\rm h}, \hat{r}_{\rm t}, \bar{\beta})$$

We consider the likelihood

$$L_{\rm tot} = L_{\rm MP}(r_0, \rho_0; \hat{R}_{\rm h}, \hat{r}_{\rm t}, \bar{\beta}) \cdot L_{\rm MR}(r_0, \rho_0; \hat{R}_{\rm h}, \hat{r}_{\rm t}, \bar{\beta})$$

$$\chi_{\rm tot} = \chi^2_{\rm MP} + \chi^2_{\rm MR}$$

For each population

$$\chi^2 = \chi^2_{\Sigma} + \chi^2_{\sigma}$$

$$\chi^2_{\rm MP} = \chi^2_{\Sigma} + \chi^2_{\sigma} + \chi^2_{r_{\rm t}}$$

Cored Halo

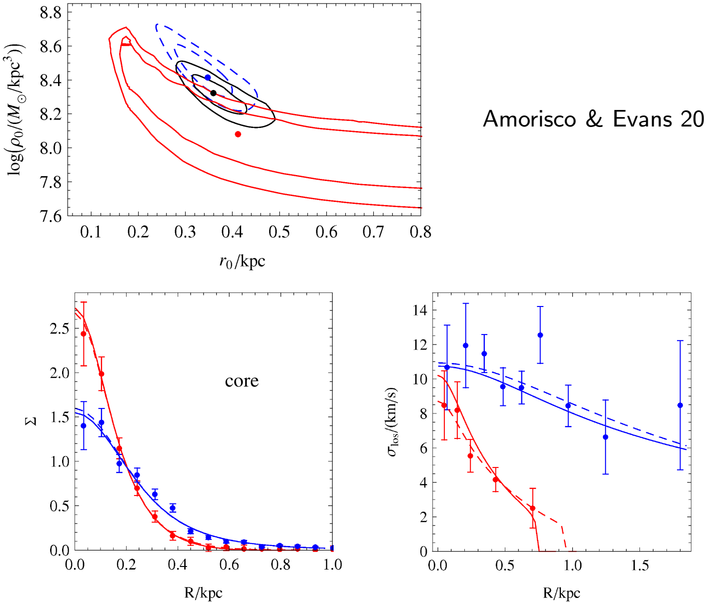

Amorisco & Evans 2012

Cusped Halo

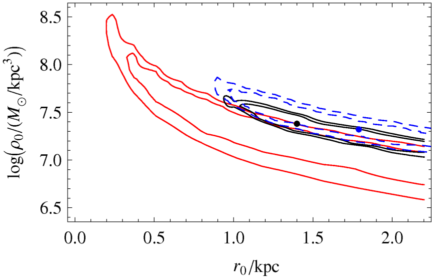

$$\Delta\chi^2_{tot} \approx 12$$

$$c \lesssim 17$$

r^{-1}-cusp 99.95%

$r^{-0.5}$-cusp 98.6%

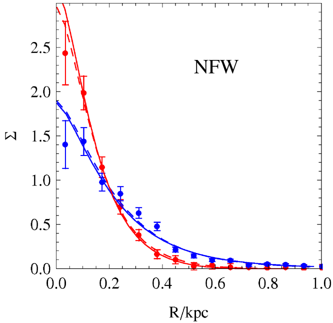

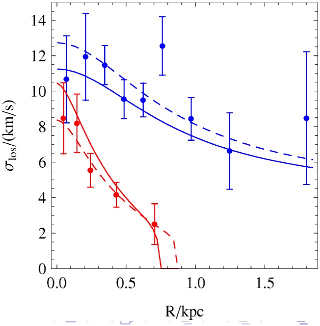

Mass Profile

Both NFW halo and cored halo have approximately the same mass profile in the range

$$200\text{pc} \leq r \leq 1.2\text{kpc}$$

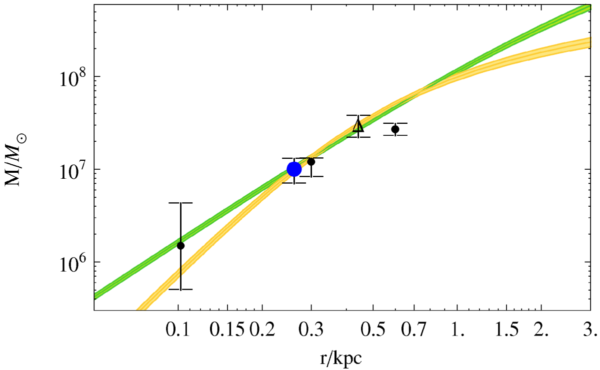

Cores from the Virial Theorem

$$\left.\begin{array}{l} \color{blue}{\mathrm{MP}}\ 2K_{los} + W_{los} = 0 \\ \color{red}{\mathrm{MR}}\ 2K_{los} + W_{los} = 0 \end{array}\right\}$$ both populations satisfy the Virial Theorem

$$K_{los} \propto \int_0^\infty RdR\ \Sigma_*\ \sigma_{los}^2$$

$$W_{los} \propto \int_0^\infty RdR\ \Sigma_* \int_0^R r^2 dr\ \frac{\rho_{dm}}{\sqrt{R^2 - r^2}}$$

A fundamental constrain
based on measured quantities only:
no dependence on the orbital structure β!

Agnello & Evans 2012

Cores from the Virial Theorem

$$\rho_{dm} = \rho_0 \ (\epsilon^2 + r^2/r_s^2)^{-1/2}(1 + r^2/r_s^2)$$

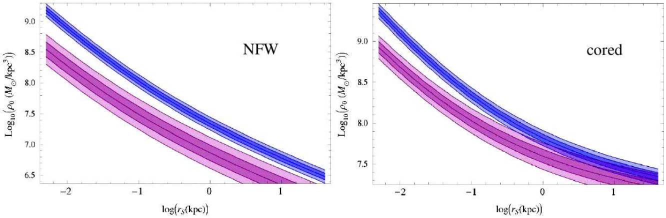

- Deviations from spherical symmetry
- Self-gravity contributions

Any core smaller than $\approx 120\text{pc}$
is not compatible (less than 2σ) with the VT.

Agnello & Evans 2012

Line Profiles

- Line Profiles constrain the orbital structure;
- break degeneracies: mass profile at the center and at large radii;
- constrain feasible formation scenarios.

LOSVDs are usually assumed to be Gaussians. Deviations are measured by using Gauss-Hermite expansions.

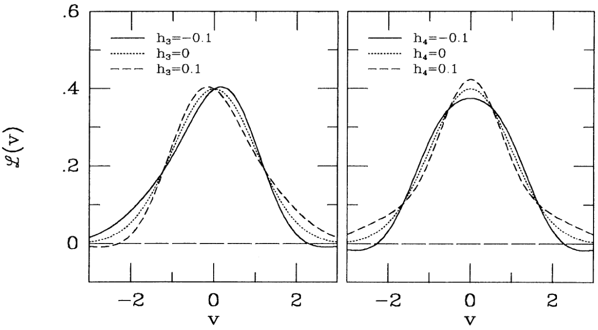

Gerhard 1993, van der Marel & Franx 1993

Issues with Discrete Data

- Gauss-Hermite series are best suited for continuous data;
- non-uniform observational uncertainties;
- limited sampling limits the accuracy.

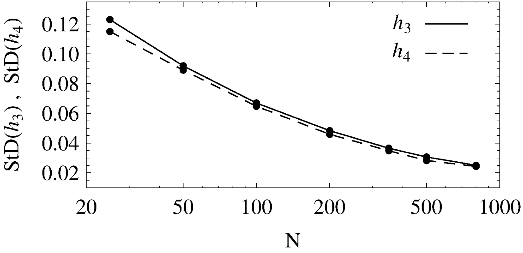

Accuracy Limits: Standard Deviation for h_3 and h_4 at sample size N.

For N smaller than 200,
noise may be larger than expected signal.

Issues with Discrete Data

- Gauss-Hermite series are best suited for continuous data;
- non-uniform observational uncertainties;
- limited sampling limits the accuracy.

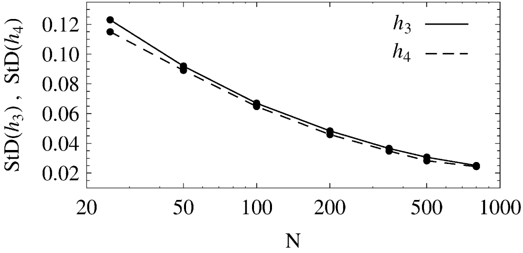

Accuracy Limits: Standard Deviation for h_3 and h_4 at sample size N.

For N smaller than 200,
noise may be larger than expected signal.

Issues with Discrete Data

A tracer $v_i \pm \delta_i$ is associated with the velocity distribution $\mathscr{L} * \mathscr{G}(\delta_i)$, rather than with the intrinsic $\mathscr{L}$.

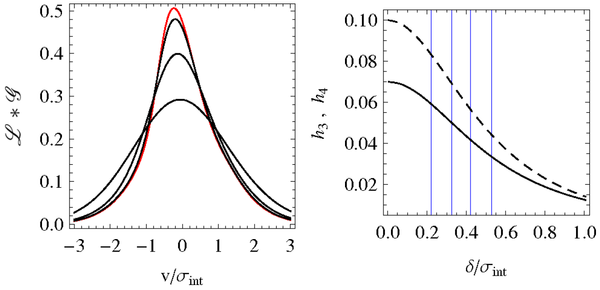

Attenuation by observational uncertainties.

On the contrary, a Bayesian implementation directly measures the intrinsic distribution $\mathscr{L}$.

Issues with Discrete Data

A tracer $v_i \pm \delta_i$ is associated with the velocity distribution $\mathscr{L} * \mathscr{G}(\delta_i)$, rather than with the intrinsic $\mathscr{L}$.

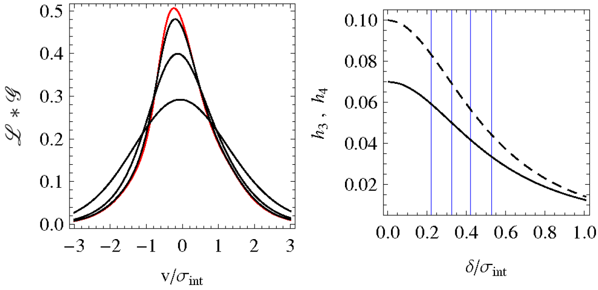

Attenuation by observational uncertainties.

On the contrary, a Bayesian implementation directly measures the intrinsic distribution $\mathscr{L}$.

A Bayesian Framework

Using all available information

- the velocities v_i;
- the uncertainties δ_i;
- the probabilities of membership p_i.

$$L(\vec{\Theta}) = \prod_{i=1}^{N} p_i \left[\mathscr{L}(\vec{\Theta}) * \mathscr{G}(\delta_i) \right] (v_i)$$

$$\vec{\Theta} = \{\mu, \sigma\} \cup \vec{\Theta}_{\mathrm{sh}} = \{\mu, \sigma, s, a\}$$

- no binning in velocity space;
- reliable uncertainties for any parameter;
- intrinsic distribution $\mathscr{L}$ recovered.

Amorisco & Evans 2012

A Bayesian Framework

Using all available information

- the velocities v_i;
- the uncertainties δ_i;
- the probabilities of membership p_i.

$$L(\vec{\Theta}) = \prod_{i=1}^{N} p_i \left[\mathscr{L}(\vec{\Theta}) * \mathscr{G}(\delta_i) \right] (v_i)$$

$$\vec{\Theta} = \{\mu, \sigma\} \cup \vec{\Theta}_{\rm sh} = \{\mu, \sigma, s, a\}$$

- no binning in velocity space;
- reliable uncertainties for any parameter;
- intrinsic distribution $\mathscr{L}$ recovered.

Amorisco & Evans 2012

Symmetric deviations: s

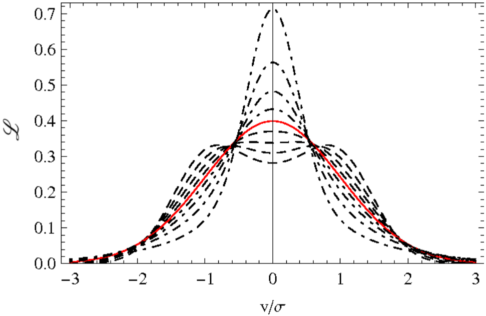

The symmetric distributions: $\mathscr{L}(s; v)$.

Constructed by using the simple model

$$f(v_r, |\vec{v}_t|) \propto |\vec{v}_t|^{-2s} \exp\left[-\frac{v_r^2 + |\vec{v}_t|^2}{2\sigma_r^2}\right]$$

with anisotropy $\beta = s$ and los direction $\varphi(s)$.

Asymmetric deviations: a

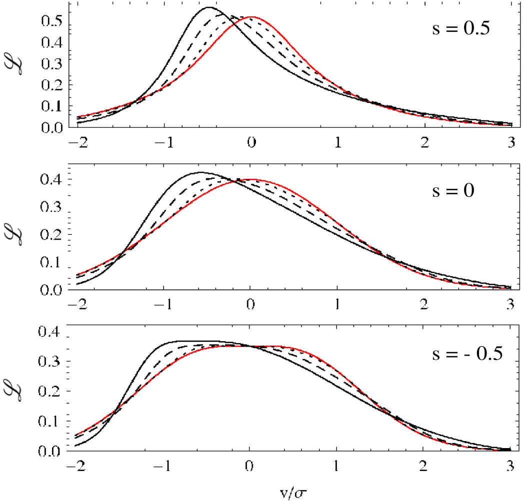

Asymmetry is driven by a suitable tranformation of the symmetric family:

$$\mathscr{L}(s,a;v) \equiv \mathscr{L}(s;X(s,a;v))$$

The asymmetric distributions: $\mathscr{L}(s,a;v)$.

Performance

Does it work any better?

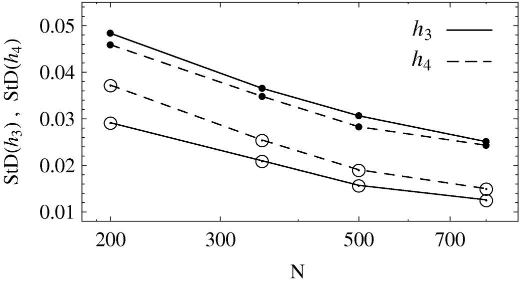

Comparing Accuracy: Standard Deviation for h_3 and h_4 at a given sample size N.

The relative gain in accuracy is significant even with no observational uncertainties or probabilities of membership.

Assessing Statistical Significance

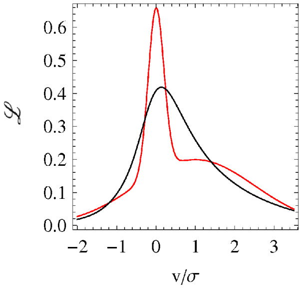

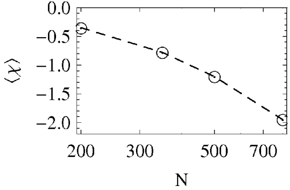

What if this family is not general enough?

Comparing the maximum likelihood

$$\bar{L} = \prod_{i=1}^{N} p_i \left[\mathscr{L}(\vec{\Theta}) * \mathscr{G}(\delta_i) \right] (v_i)$$

with the *average* likelihood for the same parameters

$$\langle \prod_{i=1}^{N} p_i \ \mathscr{L} * \mathscr{G} \rangle = \prod_{i=1}^{N} p_i \int \left[\mathscr{L} * \mathscr{G}(\delta_i) \right]^2$$

and the natural scatter induced by sample size

$$\chi = \left(\bar{L} - \langle L \rangle \right) / \mathrm{StD} \left[\langle L \rangle \right]$$

Carina dSph

758 giants with $p_i \geq 0.9$; $\langle\delta\rangle/\sigma \approx 0.53$

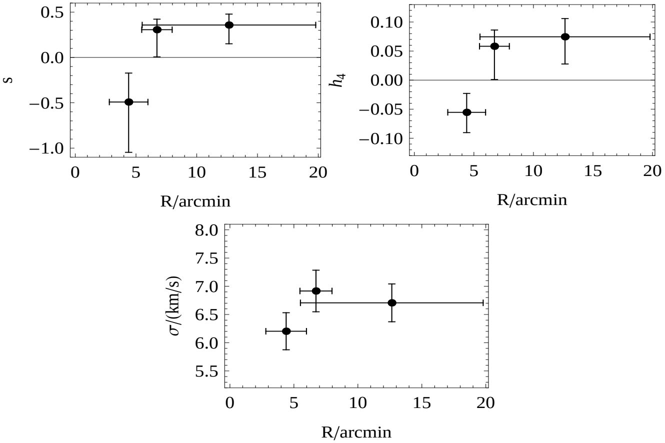

Profiles in circular annuli for the Carina dSph; $R_h \approx 8.2$arcmin. Data from Walker et al. 2009.

Sextans dSph

424 giants with $p_i \geq 0.9$; $\langle\delta\rangle/\sigma \approx 0.42$

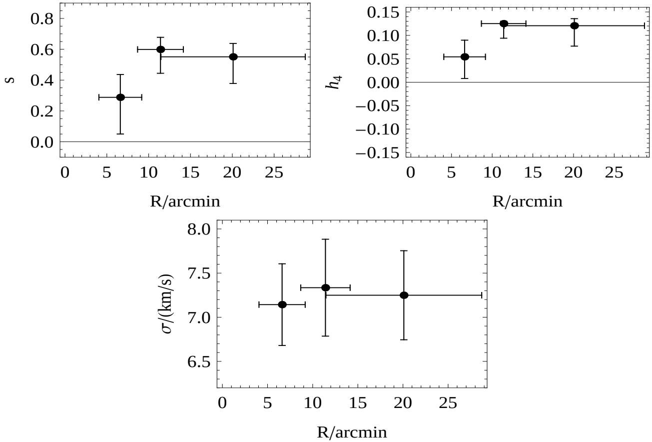

Profiles in circular annuli for the Sextans dSph; $R_{core} \approx 16.6$arcmin. Data from Walker et al. 2009.

Sculptor dSph

1355 giants with $p_i \geq 0.9$; $\langle\delta\rangle/\sigma \approx 0.33$

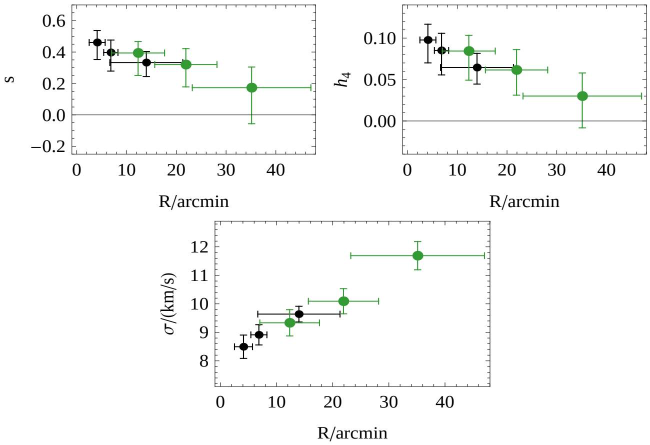

Profiles in circular annuli for the Sculptor dSph; $R_h \approx 11.3$arcmin. Data from Starkenburg et al. 2010 in green.

Fornax dSph

2409 giants with $p_i \geq 0.9$; $\langle\delta\rangle/\sigma \approx 0.22$

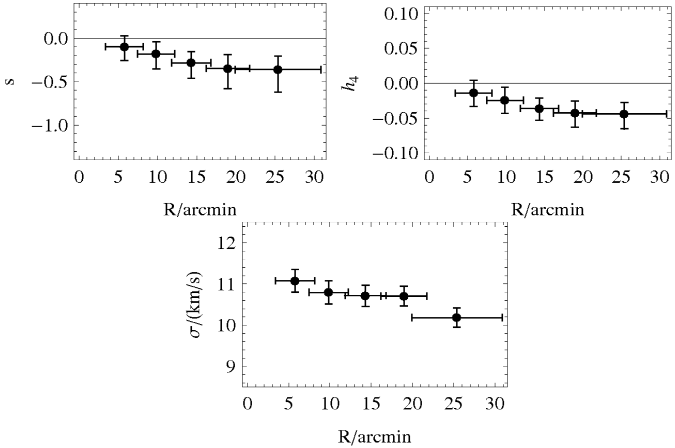

Profiles in circular annuli for the Fornax dSph; $R_h \approx 16.6$arcmin. Data from Walker et al. 2009.

Conclusions

- Detailed modelling can tackle the **dynamical structure** of dSphs
- **Multiple-pop.** systems allow to probe the presence of cusps
- Phase-Space modelling of both photometric and kinematic data in Sculptor **exclude an NFW halo**
- This result is confirmed by **different analyses**, by using **different data**
- A Bayesian framework for measuring **line profiles** allows to double accuracy
- **Sextans, Carina and Sculptor** have LOSVD more peaked than Gaussian, suggesting some radial anisotropy
- **Fornax** is the only system with flat-topped LOSVDs
- Modelling that use **all observables** is required

Mass Estimator

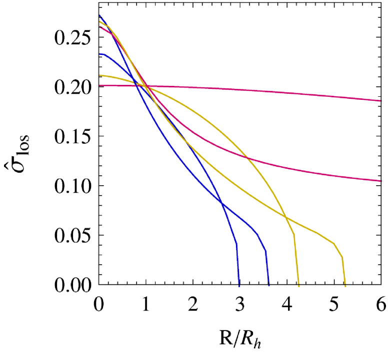

NFW halo

$$R_{\rm h}/r_0 = 0.3$$

$$M\left[(1.67 \pm 0.04)R_{\rm h}\right] = (5.85 \pm 0.2)\frac{R_{\rm h}\sigma_{\rm los}(R_{\rm h})^2}{G}$$

Independent Populations - Core

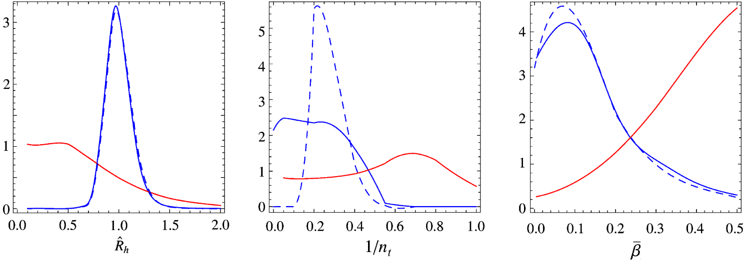

- MP: quasi isothermal, $R_{\mathrm{h},1} \approx r_0$, $\chi^2 = 40$
- MR: signs of truncation, radially anisotropic, $R_{\mathrm{h},2}$ undetermined, $\chi^2 = 2.1$

Independent Populations - NFW

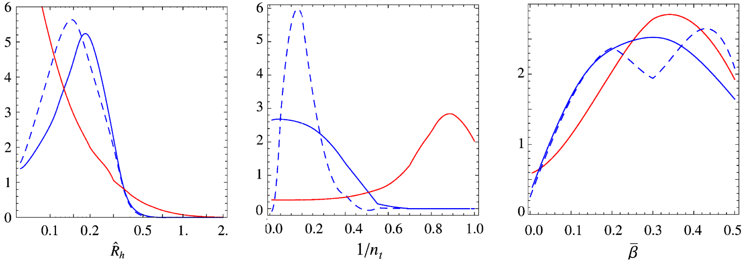

- MP: mildly radial , $R_{\mathrm{h},1} < 0.25r_0$, $\chi^2 = 49$
- MR: strongly truncated, radially anisotropic, $R_{\mathrm{h},2}$ undetermined, $\chi^2 = 3.4$

$$\left(\frac{R_{\rm h,2}}{R_{\rm h,1}}\right)^{\delta} \leq \left(\frac{\sigma_{\rm los,2}(R_{\rm h,2})}{\sigma_{\rm los,1}(R_{\rm h,1})}\right)^{2}$$

$$\Gamma = \frac{\ln\left[M(\lambda R_{\rm h,2})/M(\lambda R_{\rm h,1})\right]}{\ln\left(R_{\rm h,2}/R_{\rm h,1}\right)}$$

If $k_R \geq k_\sigma$, then

$$\Gamma = 1 + 2\frac{\ln k_\sigma}{\ln k_R} \geq \delta + 1$$

which is incompatible with $\rho \sim r^{\delta-2}$

	χ^2_Σ	$\chi^2_\Sigma + \chi^2_\sigma$	$\chi^2_\Sigma + \chi^2_\sigma + \chi^2_{r_t}$
NFW	39.3, 41.5, 45.7	48.2, 66.9, 68.3	49.0, 67.8, 69.7
cored	32.7, 36.3, 39.7	39.0, 54.3, 59.6	40.3, 55.7, 60.5
NFW	2.3, 5.6, 9.1	3.4, 11.1, 13.8	-
cored	1.1, 3.3, 4.9	2.1, 6.8, 9.9	-

Table: Results of the independent analysis of the metal-poor (upper) and metal-rich (lower) stellar component. The table gives the values of the χ^2-quantities referring, in order, to the best fit models, to the 68% and to the 95% confidence regions.

Disentangling Populations

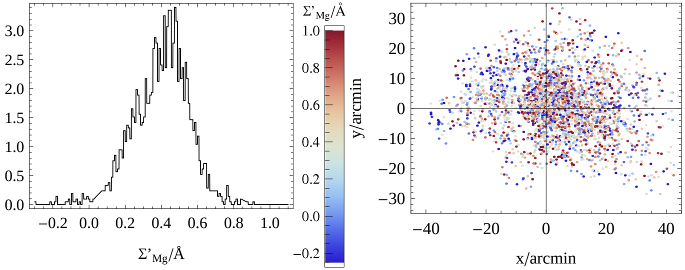

Figure: Metallicity distribution in the Fornax dSph.

$$L = \prod_{i=1}^{N} \left[\sum_j f_j \; p_{R,j}(R_i) \; p_{\Sigma,j}(\Sigma_i) \right]$$

- Plummer density profiles
- Gaussian metallicity distributions

MR - Intermediate - MP

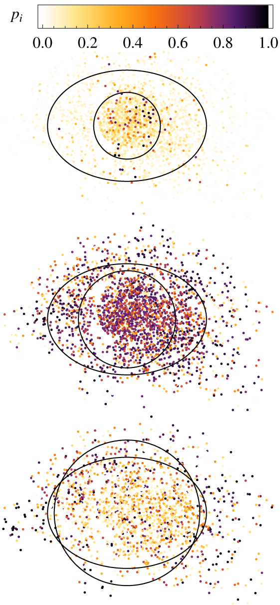

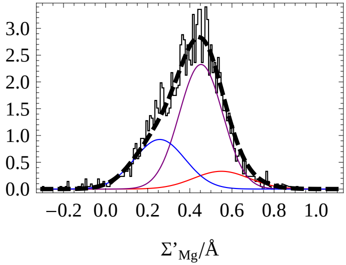

- MR: $R_h \approx 10.5$arcmin, $\langle \Sigma'_{Mg} \rangle \approx 0.55$Å, $f \approx .1$
- Int: $R_h \approx 15.3$arcmin, $\langle \Sigma'_{Mg} \rangle \approx 0.45$Å, $f \approx .6$
- MP: $R_h \approx 23$arcmin, $\langle \Sigma'_{Mg} \rangle \approx 0.26$Å, $f \approx .3$

Kinematics

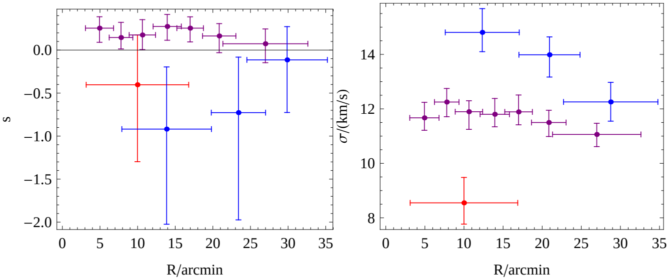

Figure: Kinematics of the disentangled populations.

...and Counter-Rotation

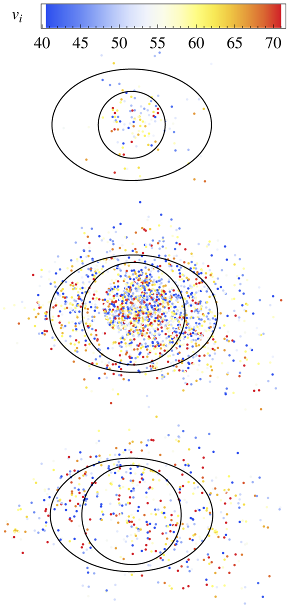

$$L_j = \prod_{i=1}^{N} p_i e^{\frac{\left[v_i - (v_{sys,j} + \Omega_{MA,j} x_i + \Omega_{ma,j} y)\right]^2}{-2\sigma_j^2}}$$

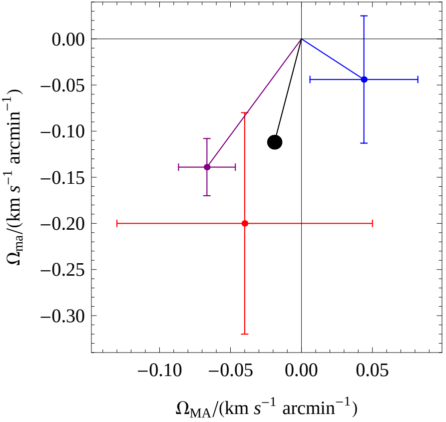

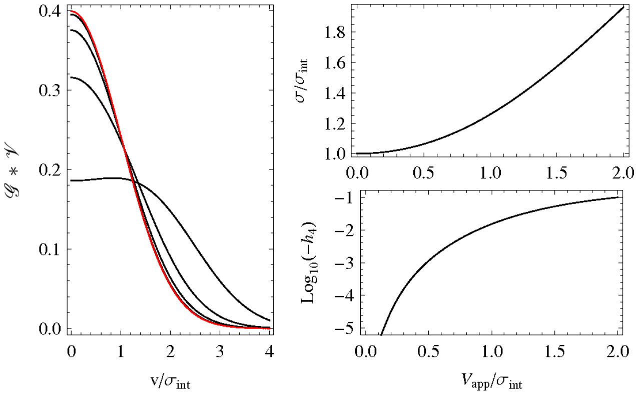

Figure: The effect of apparent rotation on circular annuli.

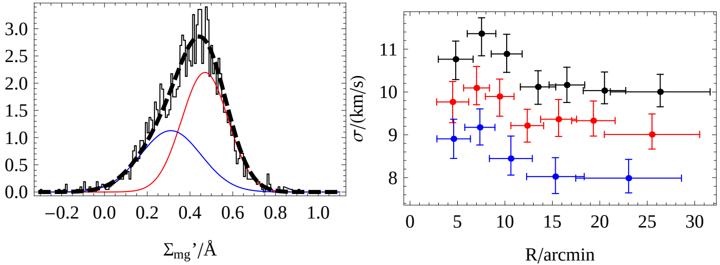

Figure: 'Unstable' kinematics for the 2-pop division in the Fornax dSph.

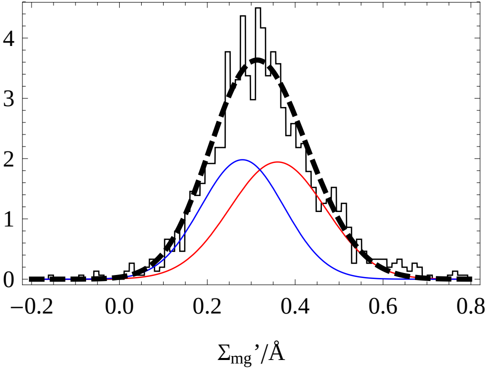

Figure: Metallicity distribution in the Sculptor dSphs.